

**DENSITY FUNCTIONAL THEORY INVESTIGATION ON THE
ELECTRONIC STRUCTURES, DYNAMICS, AND HYPERFINE
INTERACTIONS OF MUONIATED TETRAPHENYL DERIVATIVES**

TOH PEK LAN

UNIVERSITI SAINS MALAYSIA

2013

**DENSITY FUNCTIONAL THEORY INVESTIGATION ON THE
ELECTRONIC STRUCTURES, DYNAMICS, AND HYPERFINE
INTERACTIONS OF MUONIATED TETRAPHENYL DERIVATIVES**

by

TOH PEK LAN

Thesis submitted in fulfillment of the requirements

For the degree of

Doctor of Philosophy

July 2013

ACKNOWLEDGEMENT

I would like to make grateful acknowledgement to the following people:

1. My supervisors, Associate Professor Dr. Shukri Bin Sulaiman and Associate Professor Dr. Mohamed Ismail Bin Mohamed Ibrahim for their continuous supervision and guidance.
2. Dr. Jayasooriya A. Upali who had provided helpful comments with the various aspects of the work.
3. MyPhD Scholarship, Ministry of Higher Education, Malaysia.
4. My family for their support and encouragement.

TABLES OF CONTENTS

ACKNOWLEDGEMENT	ii
TABLES OF CONTENTS	iii
LIST OF TABLES	vii
LIST OF FIGURES	x
LIST OF ABBREVIATIONS	xxi
ABSTRAK	xxii
ABSTRACT	xxiv
CHAPTER 1 – INTRODUCTION	1
1.1 Introduction	1
1.2 Problem Statement	4
1.3 Objective	5
1.4 Outline of the Thesis	5
1.5 Choice of Cluster	6
CHAPTER 2 – LITERATURE REVIEW	15
2.1 Positive Muon and Muonium in Chemistry	15
2.2 Introduction to μ SR Techniques	17
2.3 Theoretical Calculations	19
2.3.1 Schrödinger Equation	19
2.3.2 Born Oppenheimer Approximation	21
2.3.3 Density Functional Theory	22

2.3.4	Basis Set	27
2.3.5	Muonium Hyperfine Interactions	29
2.3.6	Vibrational Averaging	31
2.4	Mulliken Population Analysis	33
2.5	Intermolecular Interactions	36
2.6	Rotational Energy Barrier	37
CHAPTER 3 – METHODOLOGY		40
3.1	Pure System	44
3.1.1	Simple Molecular System	45
3.1.1.1	Benzene	45
3.1.1.2	Tetraphenyl Derivatives	47
3.1.2	Rotational Dynamics of the Single Molecule	47
3.1.3	Intermolecular Interactions Effect on the Large Molecular Cluster	51
3.1.4	Rotational Dynamics of the Large Molecules	55
3.2	Muoniated System	55
3.2.1	Small Molecular Cluster	55
3.2.1.1	Muoniated Benzene	55
3.2.1.2	Muoniated Tetraphenyl Derivatives	57
3.2.2	Rotational Dynamics of the Small Muoniated System	67
3.2.3	Large Molecular Cluster	67

3.2.4	Rotational Dynamics of the Large Muoniated System	77
CHAPTER 4 –	RESULTS AND DISCUSSION	78
4.1	Pure System	79
4.1.1	Simple Molecular System	79
4.1.1.1	Benzene	79
4.1.1.2	Tetraphenyl Derivatives	84
4.1.2	Rotational Dynamics of the Single Molecule	102
4.1.3	Intermolecular Interactions Effect on the Large Molecular Cluster	115
4.1.4	Rotational Dynamics of the Large Molecules	121
4.2	Muoniated System	131
4.2.1	Small Molecular Cluster	131
4.2.1.1	Muoniated Benzene	131
4.2.1.2	Muoniated Tetraphenylmethane	143
4.2.1.3	Muoniated Tetraphenylsilane	167
4.2.1.4	Muoniated Tetraphenylgermane	191
4.2.2	Rotational Dynamics of the Small Muoniated System	215
4.2.3	Large Molecular Cluster	247
4.2.3.1	Muoniated Tetraphenylmethane	247
4.2.3.2	Muoniated Tetraphenylsilane	268
4.2.3.3	Muoniated Tetraphenylgermane	289

4.2.4	Rotational Dynamics of the Large Muoniated System	310
CHAPTER 5 –	CONCLUSIONS AND FUTURE WORKS	352
REFERENCES		361
LIST OF PUBLICATIONS		371

LIST OF TABLES

Table 1.1	Crystallographic data for tetraphenyl derivatives	9
Table 1.2	Selected activation energy barriers in muoniated systems	13
Table 2.1	The properties of positive muon	16
Table 2.2	The properties of muonium	16
Table 3.1	Symmetry operations used to generate five nearest neighbours surrounding one of the phenyl rings in the central molecule of XPh_4	51
Table 4.1	Optimized geometrical parameters of benzene	80
Table 4.2	Calculated total and frontier molecular orbital energies (eV) of benzene	81
Table 4.3	Calculated atomic charge distribution of benzene	84
Table 4.4	Selected geometrical parameters of XPh_4	85
Table 4.5	Calculated total and frontier molecular orbitals energies (eV) of XPh_4	87
Table 4.6	Calculated atomic charge distribution of XPh_4	101
Table 4.7	Selected geometrical parameters of $(XPh_4)_6$	115
Table 4.8	Calculated total and Frontier molecular orbitals energies (eV) of $(XPh_4)_6$	116
Table 4.9	Calculated atomic charge distribution of $(XPh_4)_6$	117
Table 4.10	Geometrical parameters of muoniated benzene	132
Table 4.11	Total and frontier molecular orbital energies (eV) of muoniated benzene	135
Table 4.12	Atomic charges of muoniated benzene	140

Table 4.13	Spin densities of muoniated benzene	140
Table 4.14	Hyperfine coupling constants (MHz) of Mu adducts in benzene	143
Table 4.15	Geometrical parameters of CPh ₄ -Mu	144
Table.4.16	Total and frontier molecular orbital energies (eV) of CPh ₄ -Mu	151
Table 4.17	Atomic charges of CPh ₄ -Mu	160
Table 4.18	Spin densities of CPh ₄ -Mu	160
Table 4.19	Hyperfine coupling constants (MHz) of Mu adducts in CPh ₄	167
Table 4.20	Geometrical parameters of SiPh ₄ -Mu	168
Table.4.21	Total and frontier molecular orbital energies (eV) of SiPh ₄ -Mu	175
Table 4.22	Atomic charges of SiPh ₄ -Mu	183
Table 4.23	Spin densities of SiPh ₄ -Mu	183
Table 4.24	Hyperfine coupling constants (MHz) of Mu adducts in SiPh ₄	191
Table 4.25	Geometrical parameters of GePh ₄ -Mu	192
Table.4.26	Total and frontier molecular orbital energies (eV) of GePh ₄ -Mu	198
Table 4.27	Atomic charges of GePh ₄ -Mu	207
Table 4.28	Spin densities of GePh ₄ -Mu	207
Table 4.29	Hyperfine coupling constants (MHz) of Mu adducts in GePh ₄	214
Table 4.30	Geometrical parameters of (CPh ₄) ₆ -Mu	248
Table 4.31	Total and frontier molecular orbital energies (eV) of (CPh ₄) ₆ -Mu	255

Table 4.32	Atomic charges of (CPh ₄) ₆ -Mu	260
Table 4.33	Spin densities of (CPh ₄) ₆ -Mu	260
Table 4.34	Hyperfine coupling constants (MHz) of Mu adducts in (CPh ₄) ₆	268
Table 4.35	Geometrical parameters of (SiPh ₄) ₆ -Mu	269
Table 4.36	Total and frontier molecular orbital energies (eV) of (SiPh ₄) ₆ -Mu	276
Table 4.37	Atomic charges of (SiPh ₄) ₆ -Mu	281
Table 4.38	Spin densities of (SiPh ₄) ₆ -Mu	281
Table 4.39	Hyperfine coupling constants (MHz) of Mu adducts in (SiPh ₄) ₆	288
Table 4.40	Geometrical parameters of (GePh ₄) ₆ -Mu	290
Table 4.41	Total and frontier molecular orbital energies (eV) of (GePh ₄) ₆ -Mu	297
Table 4.42	Atomic charges of (GePh ₄) ₆ -Mu	302
Table 4.43	Spin densities of (GePh ₄) ₆ -Mu	302
Table 4.44	Hyperfine coupling constants (MHz) of Mu adducts in (GePh ₄) ₆	309

LIST OF FIGURES

Figure 1.1	Molecular structure of benzene	7
Figure 1.2	Molecular structures of tetraphenyl derivatives: (a) tetraphenylmethane, (b) tetraphenylsilane, and (c) tetraphenylgermane	10
Figure 3.1	Labelling of atoms in benzene	46
Figure 3.2	Labelling of atoms in tetraphenyl derivatives: (a) tetraphenylmethane, (b) tetraphenylsilane, and (c) tetraphenylgermane	48
Figure 3.3	Selected structures of tetraphenyl derivatives: (a) (CPh ₄) ₆ , (b) (SiPh ₄) ₆ , and (c) (GePh ₄) ₆	52
Figure 3.4	Structure of muoniated benzene	56
Figure 3.5	Single molecule of CPh ₄ cluster containing Mu trapped at the (a) <i>ortho</i> , (b) <i>meta</i> , and (c) <i>para</i> sites of a phenyl ring	58
Figure 3.6	Single molecule of SiPh ₄ cluster containing Mu trapped at the (a) <i>ortho</i> , (b) <i>meta</i> , and (c) <i>para</i> sites of a phenyl ring	61
Figure 3.7	Single molecule of GePh ₄ cluster containing Mu trapped at the (a) <i>ortho</i> , (b) <i>meta</i> , and (c) <i>para</i> sites of a phenyl ring	64
Figure 3.8	Molecular structure of CPh ₄ including Mu trapped at the (a) <i>ortho</i> , (b) <i>meta</i> , and (c) <i>para</i> sites of a phenyl ring	68
Figure 3.9	Molecular structure of SiPh ₄ including Mu trapped at the (a) <i>ortho</i> , (b) <i>meta</i> , and (c) <i>para</i> sites of a phenyl ring	71
Figure 3.10	Molecular structure of GePh ₄ including Mu trapped at the (a) <i>ortho</i> , (b) <i>meta</i> , and (c) <i>para</i> sites of a phenyl ring	74
Figure 4.1	Frontier molecular orbitals of benzene, in order of decreasing energy: (a) LUMO+8, (b) LUMO+1, (c) LUMO, (d) HOMO, (e) HOMO-1, and (f) HOMO-4	82
Figure 4.2	Calculated atomic charges of benzene	83

Figure 4.3	Frontier molecular orbitals of tetraphenylmethane, in order of decreasing energy: (a) LUMO+7 (b) LUMO+6, (c) LUMO+5, (d) LUMO+4, (e) LUMO+3, (f) LUMO+2, (g) LUMO+1, (h) LUMO, (i) HOMO, (j) HOMO-1, (k) HOMO-2, (l) HOMO-3, (m) HOMO-4, (n) HOMO-5, (o) HOMO-6, (p) HOMO-7, and (q) HOMO-18	88
Figure 4.4	Frontier molecular orbitals of tetraphenylsilane, in order of decreasing energy: (a) LUMO+7 (b) LUMO+6, (c) LUMO+5, (d) LUMO+4, (e) LUMO+3, (f) LUMO+2, (g) LUMO+1, (h) LUMO, (i) HOMO, (j) HOMO-1, (k) HOMO-2, (l) HOMO-3, (m) HOMO-4, (n) HOMO-5, (o) HOMO-6, (p) HOMO-7, (q) HOMO-16, (r) HOMO-17, (s) HOMO-18, and (t) HOMO-19	91
Figure 4.5	Frontier molecular orbitals of tetraphenylgermane, in order of decreasing energy: (a) LUMO+7 (b) LUMO+6, (c) LUMO+5, (d) LUMO+4, (e) LUMO+3, (f) LUMO+2, (g) LUMO+1, (h) LUMO, (i) HOMO, (j) HOMO-1, (k) HOMO-2, (l) HOMO-3, (m) HOMO-4, (n) HOMO-5, (o) HOMO-6, (p) HOMO-7, (q) HOMO-16, (r) HOMO-17, (s) HOMO-18, and (t) HOMO-19	94
Figure 4.6	Calculated atomic charges of tetraphenyl derivatives: (a) tetraphenylmethane, (b) tetraphenylsilane, and (c) tetraphenylgermane	98
Figure 4.7	Computed relative C ₁ -C ₂ bond lengths and energies as a function of the rotational angles in CPh ₄	103
Figure 4.8	The molecular structure of CPh ₄ , with the rotational angles of (a) 110° and (b) 290°	104
Figure 4.9	Computed relative Ge ₁ -C ₂ bond lengths and energies as a function of the rotational angles in SiPh ₄	106
Figure 4.10	The molecular structure of SiPh ₄ , with the rotational angles of (a) 120° and (b) 300°	107
Figure 4.11	Computed relative Ge ₁ -C ₂ bond lengths and energies as a function of the rotational angles in GePh ₄	109
Figure 4.12	The molecular structure of GePh ₄ , with the rotational angles of (a) 120° and (b) 300°	110
Figure 4.13	Calculated relative X-C ₂ bond lengths as a function of the	112

	rotational angles in XPh_4	
Figure 4.14	Calculated relative energies as a function of the rotational angles in XPh_4	113
Figure 4.15	Calculated atomic charges of tetraphenyl derivatives: (a) $(CPh_4)_6$, (b) $(SiPh_4)_6$, and (c) $(GePh_4)_6$	118
Figure 4.16	Computed relative C_1-C_2 bond lengths and energies as a function of the rotational angles in $(CPh_4)_6$	123
Figure 4.17	Comparison of relative C_1-C_2 bond lengths and energies between CPh_4 and $(CPh_4)_6$ clusters	124
Figure 4.18	Computed relative Si_1-C_2 bond lengths and energies as a function of the rotational angles in $(SiPh_4)_6$	125
Figure 4.19	Comparison of relative Si_1-C_2 bond lengths and energies between $SiPh_4$ and $(SiPh_4)_6$ clusters	126
Figure 4.20	Computed relative Ge_1-C_2 bond lengths and energies as a function of the rotational angles in $(GePh_4)_6$	127
Figure 4.21	Comparison of relative Ge_1-C_2 bond lengths and energies between $GePh_4$ and $(GePh_4)_6$ clusters	128
Figure 4.22	Calculated relative $X-C_2$ bond lengths as a function of the rotational angles in $(XPh_4)_6$	129
Figure 4.23	Calculated relative energies as a function of the rotational angles in $(XPh_4)_6$	130
Figure 4.24	Relationship of total energy curve with C–Mu bond length in benzene	133
Figure 4.25	Location of Mu trapped in benzene	134
Figure 4.26	Frontier molecular orbitals of muoniated benzene, with the decreasing energies of (a) LUMO+7, (b) LUMO+4, (c) LUMO, (d) HOMO, (e) HOMO–1, (f) HOMO–2, and (g) HOMO–7 orbitals	136
Figure 4.27	Molecular orbital interactions diagram illustrating the coupling of benzene and Mu in muoniated benzene	138

Figure 4.28	Atomic charges of muoniated benzene	141
Figure 4.29	Spin densities of muoniated benzene	142
Figure 4.30	Relationship of total energy curve with C–Mu bond length in CPh ₄ –Mu	145
Figure 4.31	Location of Mu adducts in CPh ₄ –Mu clusters: (a) <i>ortho</i> , (b) <i>meta</i> , and (c) <i>para</i> sites	146
Figure 4.32	Frontier molecular orbitals of CPh ₄ –Mu at <i>ortho</i> site, with the decreasing energies of (a) LUMO+2, (b) LUMO+1, (c) LUMO, (d) HOMO, (e) HOMO–1, (f) HOMO–2 orbitals	152
Figure 4.33	Frontier molecular orbitals of CPh ₄ –Mu at <i>meta</i> site, with the decreasing energies of (a) LUMO+2, (b) LUMO+1, (c) LUMO, (d) HOMO, (e) HOMO–1, (f) HOMO–2 orbitals	153
Figure 4.34	Frontier molecular orbitals of CPh ₄ –Mu at <i>para</i> site, with the decreasing energies of (a) LUMO+2, (b) LUMO+1, (c) LUMO, (d) HOMO, (e) HOMO–1, (f) HOMO–2 orbitals	154
Figure 4.35	Molecular orbital interactions diagram illustrating the coupling of CPh ₄ and Mu in CPh ₄ –Mu clusters: (a) <i>ortho</i> , (b) <i>meta</i> , and (c) <i>para</i> sites	156
Figure 4.36	Atomic charges of CPh ₄ –Mu clusters: (a) <i>ortho</i> , (b) <i>meta</i> , and (c) <i>para</i> sites	161
Figure 4.37	Spin densities of CPh ₄ –Mu clusters: (a) <i>ortho</i> , (b) <i>meta</i> , and (c) <i>para</i> sites	164
Figure 4.38	Relationship of total energy curve with C–Mu bond length in SiPh ₄ –Mu	169
Figure 4.39	Location of Mu adducts in SiPh ₄ –Mu clusters: (a) <i>ortho</i> , (b) <i>meta</i> , and (c) <i>para</i> sites	170
Figure 4.40	Frontier molecular orbitals of SiPh ₄ –Mu at <i>ortho</i> site, with the decreasing energies of (a) LUMO+2, (b) LUMO+1, (c) LUMO, (d) HOMO, (e) HOMO–1, (f) HOMO–2 orbitals	176
Figure 4.41	Frontier molecular orbitals of SiPh ₄ –Mu at <i>meta</i> site, with the decreasing energies of (a) LUMO+2, (b) LUMO+1, (c) LUMO, (d) HOMO, (e) HOMO–1, (f) HOMO–2 orbitals	177

Figure 4.42	Frontier molecular orbitals of SiPh ₄ -Mu at <i>para</i> site, with the decreasing energies of (a) LUMO+2, (b) LUMO+1, (c) LUMO, (d) HOMO, (e) HOMO-1, (f) HOMO-2 orbitals	178
Figure 4.43	Molecular orbital interactions diagram illustrating the coupling of SiPh ₄ and Mu in SiPh ₄ -Mu clusters: (a) <i>ortho</i> , (b) <i>meta</i> , and (c) <i>para</i> sites	180
Figure 4.44	Atomic charges of SiPh ₄ -Mu clusters: (a) <i>ortho</i> , (b) <i>meta</i> , and (c) <i>para</i> sites	184
Figure 4.45	Spin densities of SiPh ₄ -Mu clusters: (a) <i>ortho</i> , (b) <i>meta</i> , and (c) <i>para</i> sites	187
Figure 4.46	Relationship of total energy curve with C-Mu bond length in GePh ₄ -Mu	193
Figure 4.47	Location of Mu adducts in GePh ₄ -Mu clusters: (a) <i>ortho</i> , (b) <i>meta</i> , and (c) <i>para</i> sites	194
Figure 4.48	Frontier molecular orbitals of GePh ₄ -Mu at <i>ortho</i> site, with the decreasing energies of (a) LUMO+2, (b) LUMO+1, (c) LUMO, (d) HOMO, (e) HOMO-1, (f) HOMO-2 orbitals	200
Figure 4.49	Frontier molecular orbitals of GePh ₄ -Mu at <i>meta</i> site, with the decreasing energies of (a) LUMO+2, (b) LUMO+1, (c) LUMO, (d) HOMO, (e) HOMO-1, (f) HOMO-2 orbitals	201
Figure 4.50	Frontier molecular orbitals of GePh ₄ -Mu at <i>para</i> site, with the decreasing energies of (a) LUMO+2, (b) LUMO+1, (c) LUMO, (d) HOMO, (e) HOMO-1, (f) HOMO-2 orbitals	202
Figure 4.51	Molecular orbital interactions diagram illustrating the coupling of GePh ₄ and Mu in GePh ₄ -Mu clusters: (a) <i>ortho</i> , (b) <i>meta</i> , and (c) <i>para</i> sites	203
Figure 4.52	Atomic charges of GePh ₄ -Mu clusters: (a) <i>ortho</i> , (b) <i>meta</i> , and (c) <i>para</i> sites	208
Figure 4.53	Spin densities of GePh ₄ -Mu clusters: (a) <i>ortho</i> , (b) <i>meta</i> , and (c) <i>para</i> sites	211
Figure 4.54	Computed relative C ₁ -C ₂ bond lengths and energies as a function of the rotational angles in CPh ₄ -Mu clusters: (a) <i>ortho</i> , (b) <i>meta</i> , and (c) <i>para</i> sites	217

Figure 4.55	Comparison of relative C ₁ -C ₂ bond lengths and energies between CPh ₄ and CPh ₄ -Mu clusters (The Mu trapped at the <i>ortho</i> position on a phenyl ring of CPh ₄ is also shown)	220
Figure 4.56	Comparison of relative C ₁ -C ₂ bond lengths and energies between CPh ₄ and CPh ₄ -Mu clusters (The Mu trapped at the <i>meta</i> position on a phenyl ring of CPh ₄ is also shown)	221
Figure 4.57	Comparison of relative C ₁ -C ₂ bond lengths and energies between CPh ₄ and CPh ₄ -Mu clusters (The Mu trapped at the <i>para</i> position on a phenyl ring of CPh ₄ is also shown)	222
Figure 4.58	Relative C ₁ -C ₂ bond lengths as a function of the rotational angles in CPh ₄ -Mu	223
Figure 4.59	Relative energies as a function of the rotational angles in CPh ₄ -Mu	224
Figure 4.60	Computed relative Si ₁ -C ₂ bond lengths and energies as a function of the rotational angles in SiPh ₄ -Mu clusters: (a) <i>ortho</i> , (b) <i>meta</i> , and (c) <i>para</i> sites	226
Figure 4.61	Comparison of relative Si ₁ -C ₂ bond lengths and energies between SiPh ₄ and SiPh ₄ -Mu clusters (The Mu trapped at the <i>ortho</i> position on a phenyl ring of SiPh ₄ is also shown)	229
Figure 4.62	Comparison of relative Si ₁ -C ₂ bond lengths and energies between SiPh ₄ and SiPh ₄ -Mu clusters (The Mu trapped at the <i>meta</i> position on a phenyl ring of SiPh ₄ is also shown)	230
Figure 4.63	Comparison of relative Si ₁ -C ₂ bond lengths and energies between SiPh ₄ and SiPh ₄ -Mu clusters (The Mu trapped at the <i>para</i> position on a phenyl ring of SiPh ₄ is also shown)	231
Figure 4.64	Relative Si ₁ -C ₂ bond lengths as a function of the rotational angles in SiPh ₄ -Mu	232
Figure 4.65	Relative energies as a function of the rotational angles in SiPh ₄ -Mu	233
Figure 4.66	Computed relative Ge ₁ -C ₂ bond lengths and energies as a function of the rotational angles in GePh ₄ -Mu clusters: (a) <i>ortho</i> , (b) <i>meta</i> , and (c) <i>para</i> sites	235

Figure 4.67	Comparison of relative Ge ₁ -C ₂ bond lengths and energies between GePh ₄ and GePh ₄ -Mu clusters (The Mu trapped at the <i>ortho</i> position on a phenyl ring of GePh ₄ is also shown)	238
Figure 4.68	Comparison of relative Ge ₁ -C ₂ bond lengths and energies between GePh ₄ and GePh ₄ -Mu clusters (The Mu trapped at the <i>meta</i> position on a phenyl ring of GePh ₄ is also shown)	239
Figure 4.69	Comparison of relative Ge ₁ -C ₂ bond lengths and energies between GePh ₄ and GePh ₄ -Mu clusters (The Mu trapped at the <i>para</i> position on a phenyl ring of GePh ₄ is also shown)	240
Figure 4.70	Relative Ge ₁ -C ₂ bond lengths as a function of the rotational angles in GePh ₄ -Mu	241
Figure 4.71	Relative energies as a function of the rotational angles in GePh ₄ -Mu	242
Figure 4.72	Calculated relative energies as a function of the rotational angles in XPh ₄ -Mu clusters: (a) <i>ortho</i> , (b) <i>meta</i> , and (c) <i>para</i> sites	244
Figure 4.73	Relationship of total energy curve with C-Mu bond length in (CPh ₄) ₆ -Mu	250
Figure 4.74	Location of Mu trapped in (CPh ₄) ₆ -Mu clusters: (a) <i>ortho</i> , (b) <i>meta</i> , and (c) <i>para</i> sites	251
Figure 4.75	Molecular orbital interactions diagram illustrating the coupling of (CPh ₄) ₆ and Mu in (CPh ₄) ₆ -Mu clusters: (a) <i>ortho</i> , (b) <i>meta</i> , and (c) <i>para</i> sites	256
Figure 4.76	Atomic charges of (CPh ₄) ₆ -Mu clusters: (a) <i>ortho</i> , (b) <i>meta</i> , and (c) <i>para</i> sites	261
Figure 4.77	Spin densities of (CPh ₄) ₆ -Mu clusters: (a) <i>ortho</i> , (b) <i>meta</i> , and (c) <i>para</i> sites	264
Figure 4.78	Relationship of total energy curve with C-Mu bond length in (SiPh ₄) ₆ -Mu	271
Figure 4.79	Location of Mu trapped in (SiPh ₄) ₆ -Mu clusters: (a) <i>ortho</i> , (b) <i>meta</i> , and (c) <i>para</i> sites	272

Figure 4.80	Molecular orbital interactions diagram illustrating the coupling of $(\text{SiPh}_4)_6$ and Mu in $(\text{SiPh}_4)_6\text{-Mu}$ clusters: (a) <i>ortho</i> , (b) <i>meta</i> , and (c) <i>para</i> sites	277
Figure 4.81	Atomic charges of $(\text{SiPh}_4)_6\text{-Mu}$ clusters: (a) <i>ortho</i> , (b) <i>meta</i> , and (c) <i>para</i> sites	282
Figure 4.82	Spin densities of $(\text{SiPh}_4)_6\text{-Mu}$ clusters: (a) <i>ortho</i> , (b) <i>meta</i> , and (c) <i>para</i> sites	285
Figure 4.83	Relationship of total energy curve with C–Mu bond length in $(\text{GePh}_4)_6\text{-Mu}$	292
Figure 4.84	Location of Mu trapped in $(\text{GePh}_4)_6\text{-Mu}$ clusters: (a) <i>ortho</i> , (b) <i>meta</i> , and (c) <i>para</i> sites	293
Figure 4.85	Molecular orbital interactions diagram illustrating the coupling of $(\text{GePh}_4)_6$ and Mu in $(\text{GePh}_4)_6\text{-Mu}$ clusters: (a) <i>ortho</i> , (b) <i>meta</i> , and (c) <i>para</i> sites	298
Figure 4.86	Atomic charges of $(\text{GePh}_4)_6\text{-Mu}$ clusters: (a) <i>ortho</i> , (b) <i>meta</i> , and (c) <i>para</i> sites	303
Figure 4.87	Spin densities of $(\text{GePh}_4)_6\text{-Mu}$ clusters: (a) <i>ortho</i> , (b) <i>meta</i> , and (c) <i>para</i> sites	306
Figure 4.88	Computed relative $\text{C}_1\text{-C}_2$ bond lengths and energies as a function of the rotational angles in $(\text{CPh}_4)_6\text{-Mu}$ clusters: (a) <i>ortho</i> , (b) <i>meta</i> , and (c) <i>para</i> sites	312
Figure 4.89	Comparison of relative $\text{C}_1\text{-C}_2$ bond lengths and energies between $\text{CPh}_4\text{-Mu}$ and $(\text{CPh}_4)_6\text{-Mu}$ clusters (The Mu trapped at the <i>ortho</i> position on a phenyl ring of $\text{CPh}_4\text{-Mu}$ and $(\text{CPh}_4)_6\text{-Mu}$, respectively is also shown)	315
Figure 4.90	Comparison of relative $\text{C}_1\text{-C}_2$ bond lengths and energies between $\text{CPh}_4\text{-Mu}$ and $(\text{CPh}_4)_6\text{-Mu}$ clusters (The Mu trapped at the <i>meta</i> position on a phenyl ring of $\text{CPh}_4\text{-Mu}$ and $(\text{CPh}_4)_6\text{-Mu}$, respectively is also shown)	316
Figure 4.91	Comparison of relative $\text{C}_1\text{-C}_2$ bond lengths and energies between $\text{CPh}_4\text{-Mu}$ and $(\text{CPh}_4)_6\text{-Mu}$ clusters (The Mu trapped at the <i>para</i> position on a phenyl ring of $\text{CPh}_4\text{-Mu}$ and $(\text{CPh}_4)_6\text{-Mu}$, respectively is also shown)	317

Figure 4.92	Comparison of relative C ₁ –C ₂ bond lengths and energies between (CPh ₄) ₆ and (CPh ₄) ₆ –Mu clusters (The Mu trapped at the <i>ortho</i> position on a phenyl ring of (CPh ₄) ₆ –Mu is also shown)	318
Figure 4.93	Comparison of relative C ₁ –C ₂ bond lengths and energies between (CPh ₄) ₆ and (CPh ₄) ₆ –Mu clusters (The Mu trapped at the <i>meta</i> position on a phenyl ring of (CPh ₄) ₆ –Mu is also shown)	319
Figure 4.94	Comparison of relative C ₁ –C ₂ bond lengths and energies between (CPh ₄) ₆ and (CPh ₄) ₆ –Mu clusters (The Mu trapped at the <i>para</i> position on a phenyl ring of (CPh ₄) ₆ –Mu is also shown)	320
Figure 4.95	Relative C ₁ –C ₂ bond lengths as a function of the rotational angles in (CPh ₄) ₆ –Mu	321
Figure 4.96	Relative energies as a function of the rotational angles in (CPh ₄) ₆ –Mu	322
Figure 4.97	Computed relative Si ₁ –C ₂ bond lengths and energies as a function of the rotational angles in (SiPh ₄) ₆ –Mu clusters: (a) <i>ortho</i> , (b) <i>meta</i> , and (c) <i>para</i> sites	324
Figure 4.98	Comparison of relative Si ₁ –C ₂ bond lengths and energies between SiPh ₄ –Mu and (SiPh ₄) ₆ –Mu clusters (The Mu trapped at the <i>ortho</i> position on a phenyl ring of SiPh ₄ –Mu and (SiPh ₄) ₆ –Mu, respectively is also shown)	327
Figure 4.99	Comparison of relative Si ₁ –C ₂ bond lengths and energies between SiPh ₄ –Mu and (SiPh ₄) ₆ –Mu clusters (The Mu trapped at the <i>meta</i> position on a phenyl ring of SiPh ₄ –Mu and (SiPh ₄) ₆ –Mu, respectively is also shown)	328
Figure 4.100	Comparison of relative Si ₁ –C ₂ bond lengths and energies between SiPh ₄ –Mu and (SiPh ₄) ₆ –Mu clusters (The Mu trapped at the <i>para</i> position on a phenyl ring of SiPh ₄ –Mu and (SiPh ₄) ₆ –Mu, respectively is also shown)	329
Figure 4.101	Comparison of relative Si ₁ –C ₂ bond lengths and energies between (SiPh ₄) ₆ and (SiPh ₄) ₆ –Mu clusters (The Mu trapped at the <i>ortho</i> position on a phenyl ring of (SiPh ₄) ₆ –Mu is also shown)	330

Figure 4.102	Comparison of relative Si ₁ –C ₂ bond lengths and energies between (SiPh ₄) ₆ and (SiPh ₄) ₆ –Mu clusters (The Mu trapped at the <i>meta</i> position on a phenyl ring of (SiPh ₄) ₆ –Mu is also shown)	331
Figure 4.103	Comparison of relative Si ₁ –C ₂ bond lengths and energies between (SiPh ₄) ₆ and (SiPh ₄) ₆ –Mu clusters (The Mu trapped at the <i>para</i> position on a phenyl ring of (SiPh ₄) ₆ –Mu is also shown)	332
Figure 4.104	Relative Si ₁ –C ₂ bond lengths as a function of the rotational angles in (SiPh ₄) ₆ –Mu	333
Figure 4.105	Relative energies as a function of the rotational angles in (SiPh ₄) ₆ –Mu	334
Figure 4.106	Computed relative Ge ₁ –C ₂ bond lengths and energies as a function of the rotational angles in (GePh ₄) ₆ –Mu clusters: (a) <i>ortho</i> , (b) <i>meta</i> , and (c) <i>para</i> sites	337
Figure 4.107	Comparison of relative Ge ₁ –C ₂ bond lengths and energies between GePh ₄ –Mu and (GePh ₄) ₆ –Mu clusters (The Mu trapped at the <i>ortho</i> position on a phenyl ring of GePh ₄ –Mu and (GePh ₄) ₆ –Mu, respectively is also shown)	340
Figure 4.108	Comparison of relative Ge ₁ –C ₂ bond lengths and energies between GePh ₄ –Mu and (GePh ₄) ₆ –Mu clusters (The Mu trapped at the <i>meta</i> position on a phenyl ring of GePh ₄ –Mu and (GePh ₄) ₆ –Mu, respectively is also shown)	341
Figure 4.109	Comparison of relative Ge ₁ –C ₂ bond lengths and energies between GePh ₄ –Mu and (GePh ₄) ₆ –Mu clusters (The Mu trapped at the <i>para</i> position on a phenyl ring of GePh ₄ –Mu and (GePh ₄) ₆ –Mu, respectively is also shown)	342
Figure 4.110	Comparison of relative C ₁ –C ₂ bond lengths and energies between (CPh ₄) ₆ and (CPh ₄) ₆ –Mu clusters (The Mu trapped at the <i>ortho</i> position on a phenyl ring of (CPh ₄) ₆ –Mu is also shown)	343
Figure 4.111	Comparison of relative C ₁ –C ₂ bond lengths and energies between (CPh ₄) ₆ and (CPh ₄) ₆ –Mu clusters (The Mu trapped at the <i>meta</i> position on a phenyl ring of (CPh ₄) ₆ –Mu is also shown)	344

- Figure 4.112 Comparison of relative C₁-C₂ bond lengths and energies 345
between (CPh₄)₆ and (CPh₄)₆-Mu clusters (The Mu trapped at
the *para* position on a phenyl ring of (CPh₄)₆-Mu is also
shown)
- Figure 4.113 Relative Ge₁-C₂ bond lengths as a function of the rotational 346
angles in (GePh₄)₆-Mu
- Figure 4.114 Relative energies as a function of the rotational angles in 347
(GePh₄)₆-Mu
- Figure 4.115 Calculated relative energies as a function of the rotational 348
angles in (XPh₄)₆-Mu clusters: (a) *ortho*, (b) *meta*, and (c)
para sites

LIST OF ABBREVIATIONS

B3LYP	Becke, 3-Parameter, Lee-Yang-Parr
CCDC	Cambridge Crystallographic Data Centre
DFT	Density Functional Theory
HOMO	Highest Occupied Molecular Orbital
LT- μ SR	Longitudinal Field Muon Spin Resonance
LUMO	Lowest Unoccupied Molecular Orbital
Mu	Muonium
NMR	Nuclear Magnetic Resonance
TF- μ SR	Transverse Field Muon Spin Rotation
XPh ₄	Tetraphenyl Derivatives
μ SR	Muon Spin Rotation/ Resonance

**PENYIASATAN TEORI FUNGSIAN KETUMPATAN KE ATAS STRUKTUR
ELEKTRONIK, DINAMIK, DAN INTERAKSI HIPERHALUS BAGI
TERBITAN TETRAFENIL TERMUONIAT**

ABSTRAK

Penyiasatan Teori Fungsian Ketumpatan telah digunakan untuk mengkaji penambahan muonium (Mu) dalam terbitan tetrafenil, XPh_4 di mana $X = C, Si,$ dan Ge . Berdasarkan keputusan ujikaji Putaran/ Resonans Spin Muon, tiga tapak yang memerangkap Mu dipertimbangkan, iaitu kedudukan *orto*, *meta*, dan *para* pada salah satu gelang fenil. Lokasi Mu yang stabil di ketiga-tiga tapak yang berlainan ditentukan dengan melakukan prosedur pengoptimuman geometri terhadap Mu yang berlampir dengan satu molekul XPh_4 . Geometri yang dioptimumkan itu kemudian digunakan untuk menilai tenaga bagi sistem serta interaksi hiperhalus bagi Mu. Mekanisma bagi dinamik yang lebih pantas dalam sistem XPh_4 -Mu juga telah dikaji. Kesan interaksi antara molekul terhadap tenaga dan interaksi hiperhalus bagi Mu di ketiga-tiga tapak yang berlainan juga telah ditentukan. Keputusan menunjukkan kewujudan minimum setempat dalam profil tenaga di ketiga-tiga tapak. Nilai-nilai minimum tenaga bagi Mu yang berada di ketiga-tiga tapak adalah hampir serupa antara satu sama lain. Pemalar gandingan hiperhalus isotropik bagi Mu telah ditentukan dengan kaedah pemurataan getaran. Untuk mengkaji halangan putaran XPh_4 -Mu, gelang fenil yang berlampir dengan Mu diputarkan pada ikatan $X-C_2$ pada selang sudut 10° . Bagi ketiga-tiga tapak tersebut, setiap profil tenaga mengandungi dua halangan. Bentuk profil serta lokasi halangan bagi tapak *orto*, *meta*, dan *para* menunjukkan ciri-ciri yang hampir serupa. Selain itu, keputusan juga menunjukkan

bahawa bagi $(XPh_4)_6-Mu$, gelang fenil yang dilampirkan oleh Mu pada tapak *orto* dan *meta* mempunyai halangan tenaga putaran lebih rendah jika berbanding dengan sistem tulen. Dengan membandingkan ketiga-tiga sistem termuoniat, keputusan menunjukkan bahawa halangan tenaga putaran memamerkan pengurangan apabila saiz jejari bagi atom pusat X bertambah. Dalam penyiasatan ini, saiz kelompok juga diperkembang dengan menggunakan enam XPh_4 molekul untuk membuat simulasi persekitaran tuan rumah tetrafenil-X. Mu kemudian ditambahkan di tapak-tapak dalam kajian ini. Bagi $(XPh_4)_6-Mu$, analisis memberikan satu kesimpulan yang sama dengan kes XPh_4-Mu . Dari aspek tenaga minimum, nilai-nilai yang dikira adalah hampir sama bagi ketiga-tiga tapak tersebut. Pemalar gandingan hiperhalus isotropi bagi Mu terperangkap di tapak *meta* adalah yang paling tinggi. Dengan membandingkan ketiga-tiga sistem termuoniat, satu kesimpulan yang timbul ialah pemalar gandingan hiperhalus isotropik bagi Mu meningkat apabila saiz jejari bagi atom pusat X bertambah. Interaksi antara molekul pada sistem termuoniat tersebut menyebabkan satu perubahan yang ketara pada pemalar gandingan hiperhalus bagi Mu. Pemalar gandingan hiperhalus isotropik bagi Mu yang terperangkap di tapak *orto* dan *meta* adalah dalam julat 2.8% – 8.1% lebih besar daripada XPh_4-Mu , manakala untuk kes *para*, nilai pemalar gandingan hiperhalus isotropik yang diperoleh 1.9% – 9.8% lebih kecil.

**DENSITY FUNCTIONAL THEORY INVESTIGATION ON THE
ELECTRONIC STRUCTURES, DYNAMICS, AND HYPERFINE
INTERACTIONS OF MUONIATED TETRAPHENYL DERIVATIVES**

ABSTRACT

Density Functional Theory investigation was performed to study the addition of muonium (Mu) in tetraphenyl derivatives, XPh_4 where $X = C, Si, \text{ and } Ge$. Based on earlier Muon Spin Rotation/ Resonance experimental results, three Mu trapping sites were considered, namely *ortho*, *meta*, and *para* positions on one of the phenyl rings. The stable location of Mu at the three distinct sites of the phenyl ring was determined by performing geometry optimization procedure utilizing a single XPh_4 molecule with an attached Mu. The optimized geometries were then used to evaluate the energy of the system, as well as the hyperfine interactions for Mu. In addition, the mechanism for the faster dynamics of the XPh_4 -Mu was also studied. The effects of intermolecular interactions on the energy and hyperfine interactions for Mu at the three distinct sites were also determined. The results showed that there exists a local minimum in the energy profile at all three positions. Furthermore, the energy minimum values corresponding to Mu at the three studied sites are very similar to one another. Vibrational averaging method was utilised to determine the hyperfine coupling constants for the Mu is from the isotropic component. In order to study the rotational barrier of the XPh_4 -Mu, the phenyl ring with the Mu attached to it was rotated about the $X-C_2$ bond at intervals of 10° . For all three sites, each energy profile exhibits two barriers. The shapes of the profiles as well as the locations of the barriers for the *ortho*, *meta*, and *para* sites show similar characteristics. In addition,

the computed results also showed that for $(\text{XPh}_4)_6\text{-Mu}$, the rotational energy barriers corresponding to Mu at the *ortho* and *meta* sites are lower as compared to the pure system. Comparison of the results for the three studied muoniated systems indicated a decrease in the rotational energy barrier as the radius of the central X atom increases. In this investigation, the cluster size was also expanded using a cluster containing six molecules of XPh_4 to simulate the tetraphenyl-X host environment. A Mu was then added to the trapping sites under study. For $(\text{XPh}_4)_6\text{-Mu}$, the analyses provide a similar conclusion as that of the $\text{XPh}_4\text{-Mu}$ case. From the energy minimum aspect, the calculated values obtained are almost identical for all three sites. The isotropic hyperfine coupling constant for the Mu trapped at the *meta* site is the highest one. By comparing all three muoniated systems, one conclusion that arises is that the isotropic hyperfine coupling constant for the Mu increases as the radius of the central X atom increases. The inclusion of intermolecular interactions on the muoniated system led to a significant change in the Mu hyperfine coupling constants. The calculated hyperfine coupling constants for the Mu trapped at both *ortho* and *meta* sites in $(\text{XPh}_4)_6$ are in the range of 2.8% – 8.1% greater than that of the $\text{XPh}_4\text{-Mu}$ ones, whereas the *para* case, the values are 1.9% – 9.8% smaller.

CHAPTER 1

INTRODUCTION

1.1 Introduction

In recent years, the group 14 tetraphenyl derivatives XPh_4 ($X = C, Si, Ge, \text{ and } Sn$) structures have been widely used as tetrahedral building blocks (Cheng *et al.*, 2010; Kang *et al.*, 2008; Kim *et al.*, 2011; Liu *et al.*, 2010; Yeh *et al.*, 2001) for molecular construction in optoelectronic materials, liquid crystals, and other applications. A large number of experimental and theoretical investigations have focused on the structures of XPh_4 , such as X-ray crystallography (Chieh, 1971; Chieh, 1972; Claborn *et al.*, 2002; Glidewell and Sheldrick, 1971; Karipides and Haller, 1972; Knop *et al.*, 2002; Robbins *et al.*, 1975; Sumsion and McLachlan, 1950), Infrared and Raman spectroscopy (Henry and Noltes, 1959; Pajzderska *et al.*, 1999; Pajzderska *et al.*, 2002; Warner *et al.*, 2000), Nuclear Magnetic Resonance (Ng *et al.*, 2005; Hanson *et al.*, 2009; Schneider-Koglin *et al.*, 1994), Muon Spin Rotation/Relaxation (μ SR) technique, and others. In this study, the coordinate data of XPh_4 (Claborn *et al.*, 2002) is obtained from the Cambridge Crystallographic Data Centre (CCDC). All five tetraphenyl-X compounds have similar structures where the central atom of X is surrounded by four phenyl rings. These compounds, in addition, were also found to crystallize in the tetragonal system space group $P\bar{4}2_1C$, and $Z = 2$.

Swanson (1958) for the first time investigated the muonium ($Mu = \mu^+e^-$) precession frequencies in a depolarization state. The analyses of precession frequency characteristics for the Mu in the noble gas compounds were also

investigated by Hughes *et al.* (1960). The Mu has been detected using μ SR spectroscopy. μ SR spectroscopic technique (Jeong, 2004; McKenzie, 1999; Nagamine, 2003; Yu, 1989) is an experiment based on the positive muons (μ^+) implanted into host material. Muon can also pick up an electron to form Mu, which is paramagnetic in its neutral charge state. Muon is an elementary particle similar to electron. In 1937, Neddermeyer and Anderson discovered the muon for the first time. Its antiparticle, antimuon (μ^-) has an opposite charge (-1) and a spin of $\frac{1}{2}$. Muon has a mass of 105.7MeVc^{-2} , which is approximately one-ninth that of the proton. Muons are unstable elementary particles, which decay with the muon mean lifetime of $2.2\ \mu\text{s}$ to produce a positron and two neutrinos. These decay products reveal important information, such as hyperfine interactions, dynamics of the radical, and others. More detailed descriptions of the Mu and μ SR techniques are publically available (Aston, 1997; Jayasooriya *et al.*, 1997; Jayasooriya, 2004; Jeong, 2004; McKenzie, 1999; Nagamine, 2003; Roduner *et al.*, 1982a; Roduner *et al.*, 1982b; Roduner *et al.*, 1984; Stride, 1995; Yu, 1989). The studies of Mu in organometallic compounds, semiconductors, and other materials have been carried in the past using μ SR spectroscopic technique. Muoniated radicals have been observed through experimental and theoretical studies. In 1982 and 1984, Roduner and his co-workers reported the results of Mu hyperfine coupling constants that yielded the Mu adducts to substituted benzene. The examples of substituted benzene are methyl-substituted benzene, fluorine-substituted benzene, and others. In μ SR experiments, the results show that for *meta* case, the Mu hyperfine coupling constants have the highest value as compared to the *ortho* and *para* cases. These experimental results are in agreement with data obtained by Aston (1997) and Stride (1995), respectively. This agreement occurs because the electron spins for *meta* case were found to have nodal

surfaces, while the molecular orbitals for the other two cases were delocalized throughout the molecular system.

In 1995, the methods of μ SR used in Stride's work were Transverse Field Muon Spin Rotation (TF- μ SR) and Longitudinal Field Muon Spin Relaxation (LF- μ SR). Based on TF- μ SR experimental results, the implantation of a positive muon into tetraphenyl-X host material yielded in the formation of Mu which was added to one of the phenyl rings. Three signals corresponding to hyperfine interactions of Mu at three distinct sites were observed. In TF- μ SR experiment, however, the strong features of noise made these signals indistinguishable. Therefore, the values of Mu hyperfine parameters have not been determined from the μ SR experiment because the exact trapping site could not be ascertained using the μ SR technique. The interesting feature of Mu addition was investigated after this test for the other substituted benzene systems (Aston, 1997; Roduner *et al.*, 1982a; Roduner *et al.*, 1982b; Roduner *et al.*, 1984; Stride, 1995), which contain the phenyl ring. The three signals that correspond to the hyperfine coupling constants of Mu at three distinct sites were examined. Though the weak signals were observed for muoniated tetraphenyl systems, the spectrum features obtained are quite similar to other muoniated systems. Based on μ SR experimental results (Aston, 1997; Jayasooriya *et al.*, 1997; Jayasooriya, 2004; Roduner *et al.*, 1982a; Roduner *et al.*, 1982b; Roduner *et al.*, 1984; Stride, 1995), the three possible Mu trapping sites are the *ortho*, *meta*, and *para* positions on one of the phenyl rings. No computational studies of Mu addition to tetraphenyl derivatives have been reported from the literature review. With the constraint of computational time, the calculation results for muoniated tetraphenyl-X (X = C, Si, and Ge) compounds were chosen to be

reported in this study. Density Functional Theory (DFT) calculations were carried out to find the location of Mu adducts in tetraphenyl derivatives. The three possible Mu trapping sites were then examined in energetics and hyperfine interactions aspects. For all three studied sites, the associated electronic structures of muoniated system were determined.

1.2 Problem Statement

The μ SR timescale shows that only one Mu added to tetraphenyl-X (X = C, Si, and Ge) host materials (Aston, 1997; Jayasooriya *et al.*, 1997; Jayasooriya, 2004; Stride, 1995). There are three possible Mu trapping sites where the Mu can attach at the *ortho*, *meta*, and *para* of the phenyl ring. The questions related to the structural and electronic properties of muoniated systems provide a good focus for the study. Below are the questions.

- [a] Where is the stable location of Mu adducts in the host material?
- [b] What are the electronic structures and its associated hyperfine interactions of the muoniated system?
- [c] What is the difference between the pure molecule and muoniated system in terms of geometrical parameters, local energy minima, HOMO-LUMO gaps, and atomic charges?
- [d] How does the inclusion of intermolecular interactions affect the electronic structures and its associated hyperfine interactions of the muoniated system?
- [e] How does the muoniated system found in experimental studies show much faster dynamics as compared to the pure molecule?

1.3 Objectives

This investigation intends to answer all questions listed above. Five objectives are set to achieve the goals of this proposal. Below are the objectives.

- [a] To find the stable location of Mu adducts in tetraphenyl derivatives.
- [b] To determine the Mu hyperfine interactions at three distinct sites.
- [c] To predict the electronic structures: geometrical parameters, local energy minima, HOMO–LUMO gaps, atomic charges, and spin densities of muoniated system.
- [d] To examine the mechanism for the faster dynamics of the muoniated system.
- [e] To study the influence of intermolecular interactions on the electronic structures of the muoniated system.

1.4 Outline of the Thesis

A brief introduction of the present work is given in Chapter 1. Literature review is then discussed in Chapter 2. In Chapter 3, all DFT calculations are carried out using the Gaussian 03 software package. The host materials reported in this study are benzene and tetraphenyl–X (X = C, Si, and Ge) compounds. For each compound, a single molecule cluster is chosen to simulate the host environment. The energetics and electronic structures of all the systems are then determined. To obtain the calculated values, which are much closer to the actual experimental results, the inclusion of intermolecular interactions in the large molecular system is considered. At this point, the tetraphenyl derivatives are chosen to be discussed in Chapter 3. For a large molecular cluster there are two problems that arise during the selection of the

cluster size, namely the limited computer capacity and computational time. Therefore, only one molecule is chosen as the central molecule and the other five molecules are added to surround one of the phenyl rings in the central molecule. The energetics and its associated electronic structures are studied. The calculated rotational energy barriers of the tetraphenyl derivatives are discussed in this investigation. Next, the use of the single molecule of benzene and tetraphenyl derivatives to simulate the host environment is explained respectively. A Mu is then added to the trapping sites for further study. Geometry optimization procedure is carried out to find the stable location of Mu. Optimized geometries are then used to determine the energetics, electronic structures, and hyperfine parameters of muoniated systems. To further the investigations, the inclusion of intermolecular interactions is also studied on the muoniated system. A cluster that contains six molecules of XPh_4 including the Mu is used to simulate the host environment. The three Mu addition positions are considered, namely the *ortho*, *meta*, and *para* positions in one of the phenyl rings. For these $(XPh_4)_6$ -Mu systems, the energetics, electronic structures, and its associated hyperfine parameters are examined. In this study, the details of rotational energy barriers in muoniated tetraphenyl systems are then discussed. In Chapter 4, the results and discussion are reported. The conclusions and suggestions for the further investigations are presented in Chapter 5.

1.5 Choice of Cluster

In Figure 1.1, benzene (Kim and Lee, 2002) has a molecular formula of C_6H_6 . This molecule has six carbon and six hydrogen atoms. Benzene can also be used as the substitute group which is attached to other atoms or molecules. There are many

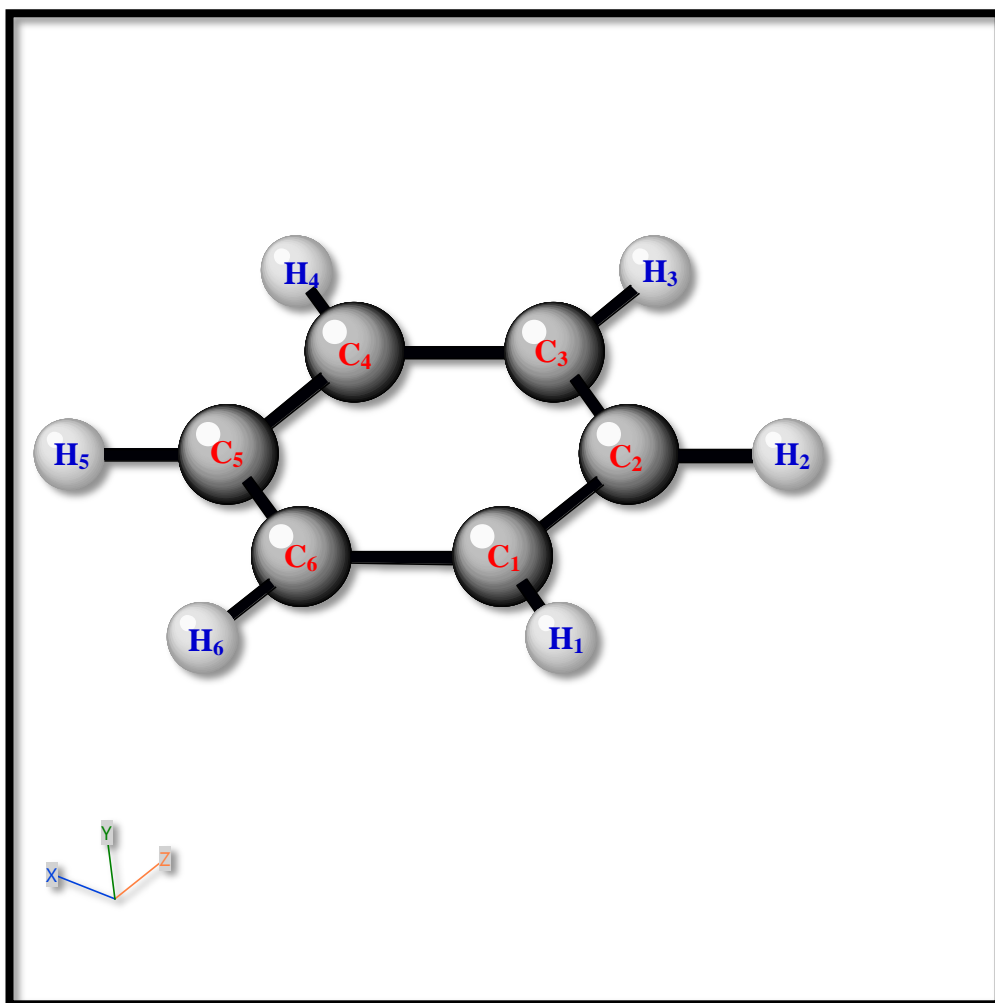


Figure 1.1: Molecular structure of benzene

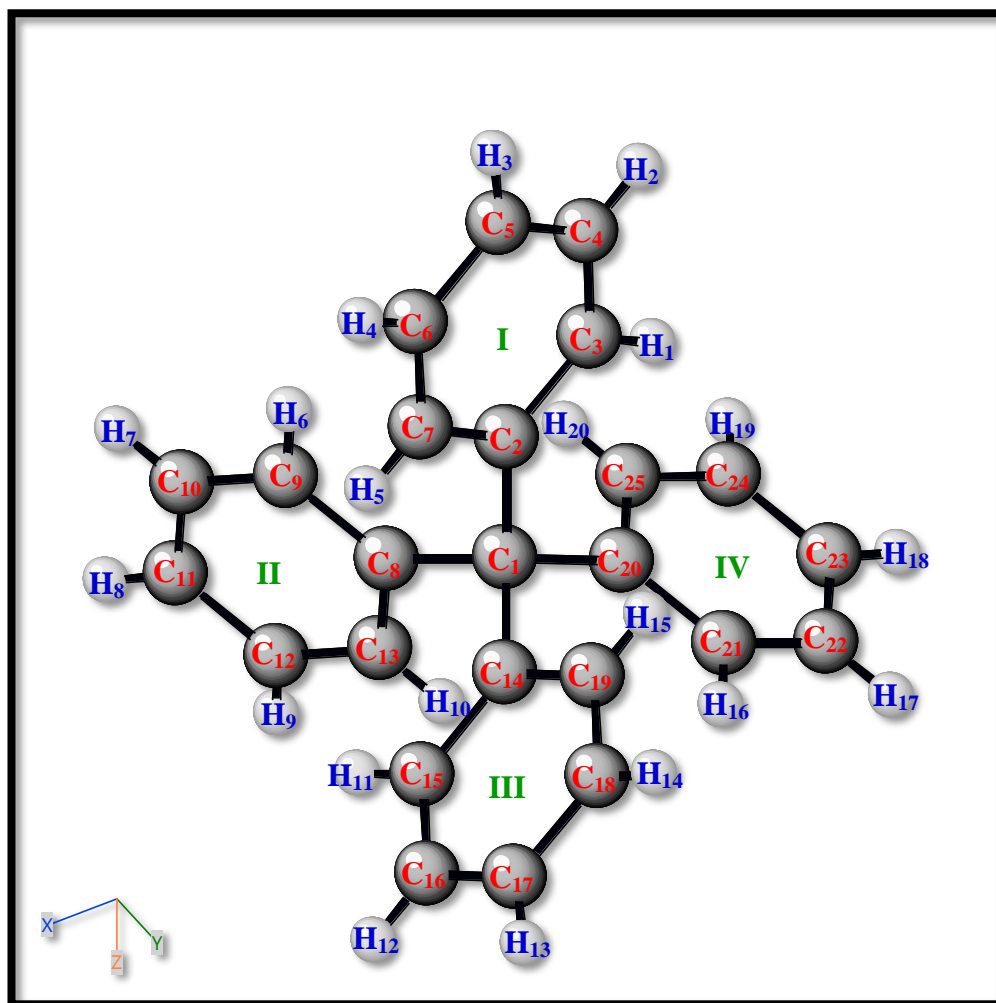
compounds containing phenyl rings, namely biphenyl, toluene, chlorobenzene, bromobenzene, fluorobenzene, benzyl fluoride, tetraphenyl-X (X = C, Si, Ge, and Sn), and others. These compounds that possess similar shape phenyl rings have different physical and chemical properties which are dependent on their shapes of molecular structures. There have been many studies recently, either theoretical or experimental, carried out on these compounds (Baker and Grant, 2006; Kim and Lee, 2002; Kubicki *et al.*, 1999; Schaefer *et al.*, 1991; Tozer, 1999). This is because these compounds can be used as building blocks for many applications. Tetraphenyl derivatives have been receiving attention in the molecular construction (Cheng *et al.*, 2010; Kim *et al.*, 2011; Liu *et al.*, 2010). These tetrahedral building blocks were successfully used as the optoelectronic materials, liquid crystals, and materials with other applications. Using the NMR technique, for example, Yeh *et al.* (2001) reported the characters of tetraphenylmethane based molecular materials, such as tetrakis(4-(5-(3,5-di-tert-butylphenyl)-2-oxadiazolyl)phenyl)methane (TBUOXD), tetrakis(4-(5-(4-diphenylaminophenyl)-2-oxadiazolyl)phenyl)methane (p-TPAOXD), and others can be used as the light emitting device. Kang *et al.* (2008) studied the tetraphenylsilane based compound, 9-(4-triphenylsilyl-(1,1',4,1'')-terphenyl-4''-yl)-9H-carbazole (TSTC). The results showed that the structure of TSTC had high LUMO level, thermal, and chemical stability, which can be used as the host for green electrophosphorescence devices.

The first observation for tetraphenylmethane (CPh₄) compound was performed by Gomberg (1898). The crystal structures of XPh₄ (X = C, Si, Ge, Sn, and Pb) were determined by X-ray crystallography (Chieh, 1971; Chieh, 1972; Claborn *et al.*, 2002; Glidewell and Sheldrick, 1971; Karipides and Haller, 1972;

Knop *et al.*, 2002; Robbins *et al.*, 1975; Sumsion and McLachlan, 1950). The results showed that all five tetraphenyl–X compounds have similar structures where the central atom of X is surrounded by four phenyl rings. These compounds were also found to crystallize in the tetragonal system, space group $P\bar{4}2_1C$, and $Z = 2$. The latest crystallographic data (Claborn *et al.*, 2002) from Cambridge Crystallographic Data Centre (CCDC) is used in this investigation. The data is summarized in Table 1.1 and the structures of XPh_4 are given in Figures 1.2(a) – 1.2(c). The anion–radicals of tetraphenylmethane (CPh_4) and tetraphenylsilane ($SiPh_4$) compounds have been studied using Electron Spin Relaxation (ESR) spectroscopic technique (Solodovnikov and Kabachnik, 1972; Il’yasov *et al.*, 1973a; Il’yasov *et al.*, 1973b). These scientists found that the spin densities were concentrated mostly on that particular ring which was attached with the alkali metal element. Using gas–phase electron diffraction (Belyakov *et al.*, 1981; Csakvari *et al.*, 1990; Campanelli *et al.*, 2001; Campanelli *et al.*, 2011), the molecular structures of tetraphenyl derivatives have been studied extensively. In 2011, Campanelli *et al.* investigated a series of organosilicon, namely diphenylsilane, triphenylsilane, and tetraphenylsilane compounds. The geometrical structures of these compounds were discussed and then compared to those of theoretical results.

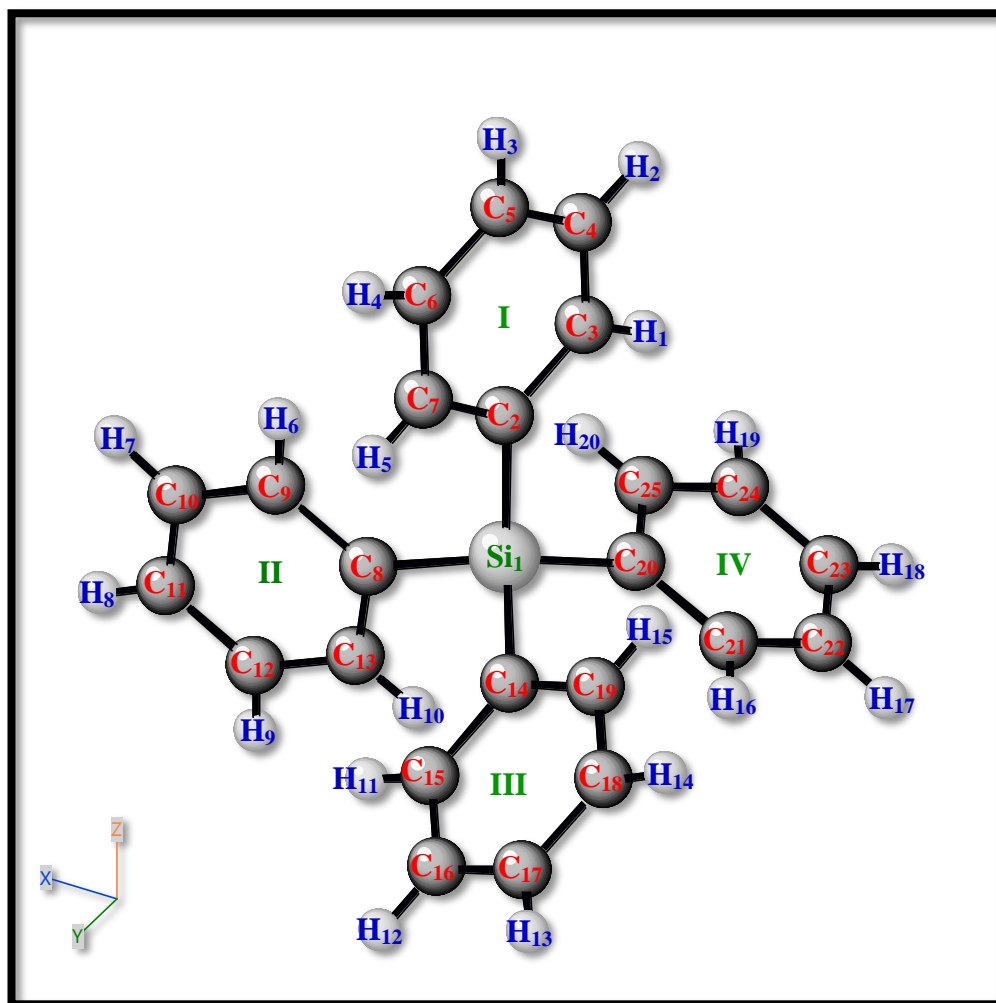
Table 1.1: Crystallographic data for tetraphenyl derivatives (Claborn *et al.*, 2002)

Host materials	CCDC reference codes	Bond lengths	Lattice parameters (Å)	
		(Å) X–C ₂	<i>a</i>	<i>c</i>
Tetraphenylmethane	TEPHME12	1.54924	10.9050(1)	7.2850(5)
Tetraphenylsilane	TEPHSI05	1.87292	11.4476(9)	7.0644(6)
Tetraphenylgermane	TEPHGE03	1.95176	11.6160(5)	6.9020(3)



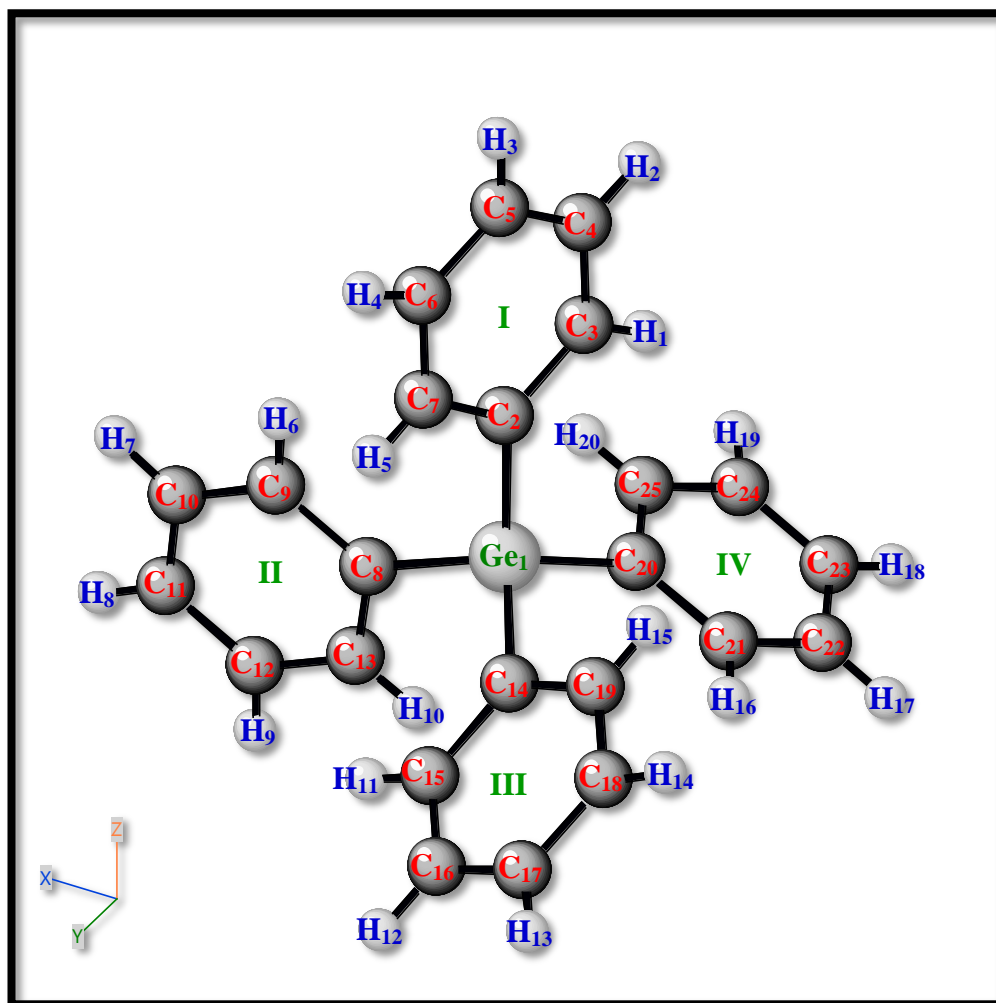
1.2(a)

Figure 1.2: Molecular structures of tetraphenyl derivatives: (a) tetraphenylmethane, (b) tetraphenylsilane, and (c) tetraphenylgermane



1.2(b)

Figure 1.2: Molecular structures of tetraphenyl derivatives: (a) tetraphenylmethane, (b) tetraphenylsilane, and (c) tetraphenylgermane



1.2(c)

Figure 1.2: Molecular structures of tetraphenyl derivatives: (a) tetraphenylmethane, (b) tetraphenylsilane, and (c) tetraphenylgermane

In addition, the molecular dynamics of tetraphenyl derivatives have also been studied using Infrared and Raman spectroscopy (Henry and Noltes, 1959; Pajzderska *et al.*, 1999; Pajzderska *et al.*, 2002; Warner *et al.*, 2000), Nuclear Magnetic Resonance (Ng *et al.*, 2005; Hanson *et al.*, 2009; Schneider–Koglin *et al.*, 1994), and others. In 1999, Pajzderska *et al.* reported that there are two kinds of molecular motions in tetraphenyltin (SnPh₄) compound, namely the reorientation of whole molecule and the rotation of phenyl ring using NMR experiments and computational DFT calculations. The Longitudinal Field Muon Spin Relaxation (LF- μ SR) study of tetraphenyl derivatives was carried out by Aston (1997) and Stride (1995). The main reason of these tetraphenyl derivatives used for the LF- μ SR study is that each XPh₄ consists of four phenyl rings, which can provide the addition sites to the Mu. The activation energy values corresponding to the rotational energy barriers of muoniated systems were examined. The activation energy barriers are summarized in Table 1.2. As seen from the table, the values of CPh₄ and SiPh₄ compounds were predicted by Stride (1995). The two samples were found to sublime easily before anything was observed experimentally. These findings of Stride (1995) were further discussed by Aston (1997) as shown in Table 1.2.

Table 1.2: Selected activation energy barriers in muoniated systems (Aston, 1997; Stride, 1995)

Host materials	Activation energies (eV)
Tetraphenylmethane	0.74 *
Tetraphenylsilane	0.37 *
Tetraphenylgermane	0.32
Tetraphenyltin	0.16

* indicates the predictions using the correlations with the radius size of central X atom.

There have been a variety of theoretical studies (Ahmed *et al.*, 1971; Chieh, 1971; Chieh, 1972; Chieh and Trotter, 1970; Glidewell and Sheldrick, 1971;

Hutchings *et al.*, 1974a; Hutchings *et al.*, 1974b; Karipides *et al.*, 1972; Knop *et al.*, 2002; Lin *et al.*, 2004; Pajzderska *et al.*, 1999; Sumsion and Mclachlan, 1950) on the electronic structures and dynamic motions of tetraphenyl derivatives. Ahmed *et al.* (1971) and Pajzderska *et al.* (1999) estimated the conformation of these compounds using the calculations of atom–atom potentials methods. The change in total energy profile was then examined and discussed. Subsequently, Campanelli *et al.* (2001; 2011) and Knop *et al.* (2002) employed the DFT method to determine the electronic structures of tetraphenylmethane and tetraphenylsilane compounds. The calculated results are in agreement with experimental values. The DFT calculations were carried out to determine the energetics of tetraphenyl derivatives (Lin *et al.*, 2004). It is of great interest to investigate these compounds with the addition of Mu using the DFT technique since a lot of the theoretical or experimental studies have been carried out for the tetraphenyl derivatives. The energetics, electronic structures, and hyperfine interactions of the mouniated system were then examined in this study.

CHAPTER 2

LITERATURE REVIEW

Chapter two presents a brief overview of previous works. A brief introduction to the concept muonium (Mu) is discussed in Sections 2.1. μ SR is the experimental technique, which uses muons as a sensitive magnetic probe of matter. Section 2.2 gives a brief introduction to the Muon Spin Rotation/ Relaxation (μ SR) technique. Some of the theoretical aspects of the thesis are discussed in Sections 2.3, 2.4, 2.5, and 2.6.

2.1 Positive Muon and Muonium in Chemistry

In 1937, Neddermeyer and Anderson discovered the muon for the first time. The muon (μ) is an elementary particle with a spin of $\frac{1}{2}$ and negative electric charge. The muon differs from the electron, where it has a mean lifetime of $2.2\mu\text{s}$. Muon only has a mass of $105.7\text{MeV}c^{-2}$, which is approximately one-ninth that of the proton. The muon can also be denoted by μ^- . This particle has an antimatter partner of opposite charge ($+e$), which can be called a positive muon (μ^+). Muons are produced by the weak decay of pions into a μ^- and μ^+ . This μ^+ can also be called as the antimuon. μ^+ is the antiparticle of a muon, where it has a lifetime of about $2.2\mu\text{s}$. μ^+ decays to positron and neutrino and antineutrino. These decay products reveal important information, such as hyperfine interactions, dynamics of the radical, and others. The properties of positive muon are presented in Table 2.1. In μ SR experiments (Aston, 1997; Jayasooriya *et al.*, 1997; Jayasooriya, 2004; McKenzie,

Table 2.1: The properties of positive muon (McKenzie, 1999)

Properties	Values
Charge	(+e)
Spin	$\frac{1}{2}$
Mass	$105.6595\text{MeV}c^{-2}$ $0.1126096m_p$
g factor	2.002331848
Mean lifetime	2.19714 μs

1999; Roduner *et al.*, 1982a; Roduner *et al.*, 1982b; Roduner *et al.*, 1984; Stadlbauer *et al.*, 1983; Stride, 1995), muons can be produced at the high energy particle acceleration. The muonium (Mu) is formed when a positive muon (μ^+) enters into the host material and captures an electron once a muon loses kinetic energy. The Mu can also be called as a light isotope of hydrogen because it has a reduced mass almost similar with the hydrogen atom. The Bohr radius of 0.531 \AA and ionization potential of 13.54 eV are almost the same with the hydrogen atom (0.529 \AA and 13.60 eV, respectively for the Bohr radius and ionization potential). Some of the Mu properties are listed in Table 2.2. Even though the muon has a short lifetime of 2.2 μs ,

Table 2.2: The properties of muonium (McKenzie, 1999)

Properties	Values
Mass	0.1131 M_H
Reduced mass	0.9956 M_H
Bohr radius	0.5315 \AA
Ionization potential	13.539 eV
Hyperfine frequency	4463 MHz in vacuum

it is long enough for a muon to be injected into the target and to make the muon stop at the any positions which can be identified using the μSR technique. This short lifetime of muon provides the information that there has never been more than one muon implanted in the sample at any given time. There have been many theoretical

studies in recent years of Mu adducts in superconductors, semiconductors, organic materials, and others (Casarin *et al.*, 1991; Magalhaes and Ramos, 1990; Oganesyana *et al.*, 2003; Scheicher *et al.*, 2006; Sulaiman, *et al.*, 1994). In one of these studies, Magalhaes and Ramos (1990) employed the Hartree Fock (HF) method to study the Mu adducts of benzene and hexafluorobenzene compounds. The geometrical parameters of muoniated systems were presented, as well as the hyperfine interactions obtained. In 2003, Oganesyana *et al.* studied the Mu adducts of DNA compounds, namely adenine, cytosine, and others. The DFT calculations were then performed to determine the associated hyperfine parameters. The calculation results presented that the hyperfine coupling constants for the Mu trapped to the carbon from the C=O group has the greatest value. These results are in agreement with other muoniated systems in the literature (Aston, 1997; Roduner *et al.*, 1982a; Roduner *et al.*, 1982b; Roduner *et al.*, 1984; Stride, 1995).

2.2 Introduction to μ SR Techniques

μ SR spectroscopic technique (Jeong, 2004; McKenzie, 1999; Nagamine, 2003; Yu, 1989) is an experiment in which the muon is implanted in the sample. The abbreviation of μ SR stands for Muon Spin Rotation/ Relaxation spectroscopy. These μ SR experiments have been carried out in several places, namely ISIS, Rutherford Appleton Laboratory in United Kingdom, TRIUMF in Canada, PSI in Switzerland, and KEK in Japan (Aston, 1997; Jayasooriya *et al.*, 1997; Jayasooriya, 2004; Nagamine, 2003; Stride, 1995; Yu, 1989). There are several advantages when using μ SR technique. First, the window time for the μ SR spectroscopy provides $\times 10^5$ times faster than NMR (http://en.wikipedia.org/wiki/Muon_spin_spectroscopy.html).

The μ SR experiments can provide a new opportunity to study the structural and magnetic phenomena in magnets, superconductors, semiconductors, insulators, organic materials, and others. As far as we know the neutron scattering experiments provide excellent results about the magnetic properties and excitation states of the magnets. However, the μ SR has a sensitive probe to determine the materials with the corresponding magnetic order, which has a short range and/ or random nature when neutron experiment fails to do so (Nagamine, 2003). Moreover, the μ SR technique does not require any radio frequency procedure to align the muon spin. Since the hydrogen atom acts as an impurity in semiconductors, the characteristic of a Mu trapping site becomes important. The analyses of low concentration semiconductor materials are difficult to perform using other spectroscopy techniques. The μ SR technique makes it possible with the unique of pions and muons decay (Jeong, 2004; McKenzie, 1999; Nagamine, 2003; Yu, 1989). This effect due to the 100% spin polarized muons can be achieved nearly at the low temperature and/ or in the strong magnetic field.

Based on μ SR experiments (Aston, 1997; Jayasooriya, *et al.*, 1997; Jayasooriya, 2004; Jeong, 2004; McKenzie, 1999; Nagamine, 2003; Stride, 1995; Yu, 1989), the collision of an accelerated proton beam with the nuclei of a production target produces positive pions. The pions decayed and positive muons were formed. The positive muon was then injected into the sample. The positive muon can also be muonium (Mu) in insulators, semiconductors, organic materials, and others. Muons are unstable particles. After the lifetime of the muon, it decays into one positron and two neutrinos. The emitted positron travels in the direction of muon spin and only this analysis of the positron provides the important information such as hyperfine

interactions, dynamics of the radicals, and others. Though the exact direction of muon spin cannot be determined by a single decay positron, the averaged direction of spin polarization for the muon ensemble can be examined using the anisotropic distribution of the decay positron from the branch of muons deposited in the same direction.

There are two types of μ SR technique configurations (Aston, 1997; Jayasooriya, 2004; McKenzie, 1999; Nagamine, 2003; Stride, 1995; Yu, 1989). In a Transverse Field Muon Spin Rotation (TF- μ SR) experiment, the applied magnetic field is set perpendicular to the spin polarization of the muon beams. Muon beams are “spin polarized”. This means that all muons experience the same applied field and spin in the same direction. TF- μ SR technique was utilized to measure the hyperfine coupling constants of Mu adducts in the sample. For the Longitudinal Field Muon Spin Relaxation (LF- μ SR) experiment, the applied field is parallel to the spin polarization of the muon beam. This technique was used to determine the activation energy value of the muoniated system.

2.3 Theoretical Calculations

2.3.1 Schrödinger Equation

In quantum mechanics, the time independent Schrödinger equation is used to obtain the energetics and electronic structures of the molecular system. The Schrödinger equation (Cramer, 2002; Gopalakrishnan, 1998; Foresman and Frisch, 1996; Jeong, 2004; Jensen, 2007; Levine, 2000) is given

$$\mathbf{H}\Psi = E\Psi \quad (2.1)$$

where

\mathbf{H} is the Hamiltonian operator for the system

E is the total energy of the system

Ψ is the wavefunction of the system

The total Hamiltonian equation for a molecular system can be written in atomic unit.

$$\begin{aligned} \mathbf{H}_{total} &= -\sum_{i=1}^N \frac{1}{2} \nabla_i^2 - \sum_{A=1}^M \frac{1}{2M_A} \nabla_A^2 - \sum_{i=1}^N \sum_{A=1}^M \frac{Z_A}{|\mathbf{R}_A - \mathbf{r}_i|} + \sum_{i=1}^N \sum_{j>i}^N \frac{1}{|\mathbf{r}_i - \mathbf{r}_j|} + \sum_{A=1}^M \sum_{B>A}^M \frac{Z_A Z_B}{|\mathbf{R}_A - \mathbf{R}_B|} \\ \mathbf{H}_{total} &= -\sum_{i=1}^N \frac{1}{2} \nabla_i^2 - \sum_{A=1}^M \frac{1}{2M_A} \nabla_A^2 - \sum_{i=1}^N \sum_{A=1}^M \frac{Z_A}{r_{iA}} + \sum_{i=1}^N \sum_{j>i}^N \frac{1}{r_{ij}} + \sum_{A=1}^M \sum_{B>A}^M \frac{Z_A Z_B}{R_{AB}} \end{aligned} \quad (2.2)$$

where

A and B are run over the M nuclei in the system

i and j are run over the N electrons in the system

$$\nabla_i^2 = \frac{\partial^2}{\partial x^2} + \frac{\partial^2}{\partial y^2} + \frac{\partial^2}{\partial z^2} \text{ is the Laplacian operator} \quad (2.3)$$

Z_A is an atomic number of the nucleus A

r_{iA} is the distance between A th nucleus and i th electron

r_{ij} is the distance between i th electron and j th electron

R_{AB} is the distance between A th nucleus and B th nucleus

M_A is the ratio of the mass of nucleus A to the electron mass

For the molecular Hamiltonian equation in (2.2), the first term is the operator for the kinetic energy of the electrons, the second term is the operator for the kinetic energy of the nuclei, the third term is the attraction potential energy between the electron and nucleus, the fourth term is the repulsion potential energy between the electrons, and the last term is the repulsion potential energy between the nuclei.

2.3.2 Born Oppenheimer Approximation

The Hamiltonian equation in (2.2) is difficult to solve the molecular system even for a small molecule. Born Oppenheimer (BO) approximation (Cramer, 2002; Gopalakrishnan, 1998; Foresman and Frisch, 1996; Jeong, 2004; Jensen, 2007; Levine, 2000) is used to simplify the total Hamiltonian of a molecular system by separating the electronic and nuclear motions. It consists of two parts. For the first part of BO approximation, it is only used to simplify the electronic Hamiltonian equation. The electronic Hamiltonian equation is written as

$$\mathbf{H}_{electronic} = -\sum_{i=1}^N \frac{1}{2} \nabla_i^2 - \sum_{i=1}^N \sum_{i=A}^M \frac{Z_A}{r_{iA}} + \sum_{i=1}^N \sum_{j>i}^N \frac{1}{r_{ij}} \quad (2.4)$$

The electronic Schrödinger equation is given by

$$\mathbf{H}_{electronic} \Psi_{electronic}(r, R_{AB}) = E_{electronic}(R_{AB}) \Psi_{electronic}(r, R_{AB}) \quad (2.5)$$

where

$E_{electronic}(R_{AB})$ is the electronic energy of the system

$\Psi_{electronic}(r, R_{AB})$ is the electronic wavefunction of the system

For the second part, the BO approximation is used to re–present the kinetic energy of the nuclei. As the electrons move much faster than the nuclei, the electronic coordinates are replaced by their averaged values, averaged over their electronic functions. This step of the BO approximation involves the separation of vibrational, rotational, and translational motions of the nuclei. The nuclear Hamiltonian equation is given as

$$\mathbf{H}_{nuclear} = -\sum_{A=1}^M \frac{1}{2M_A} \nabla_A^2 + E_{total}(R_{AB}) \quad (2.6)$$

The total energy of the system is the sum of an electronic energy and nuclear repulsion potential energy.

$$E_{total}(R_{AB}) = E_{electronic}(R_{AB}) + \sum_{A=1}^M \sum_{B>A}^M \frac{Z_A Z_B}{R_{AB}} \quad (2.7)$$

Note: This influence of nuclear motion will be used to discuss the vibrational averaging for the muon in Section 2.3.6.

2.3.3 Density Functional Theory

Density functional theory (DFT) is the most popular computational method used to investigate the electronic structures in a molecular system. In recent years, the DFT calculations have been widely employed in the solid–state systems because of many cases the results of DFT calculation agree quite satisfactorily with experimental data. From the literature survey, there are a lot of functionals available (Sousa, *et al.*, 2007). B3LYP is one of the popular DFT functionals. In this study, B3LYP is the functional employed for our calculations. In order to study the functional of B3LYP,

the basic principles of DFT (Cramer, 2002; Foresman and Frisch, 1996; Jensen, 2007; Levine, 2000) are discussed in detail. In the literature, the DFT method is utilized to calculate the molecular energy from the aspect of electron density, ρ . In 1964, the foundation for DFT has been proved by Hohenberg and Kohn. The first theorem of Hohenberg–Kohn model states that the ground state energy of a molecular system is a unique functional of the electron density.

$$E_0 = E(\mathbf{r}) \quad (2.8)$$

The second theorem establishes that the functional $E(\mathbf{r})$ has its energy minimum relative to the variation $\delta\rho(\mathbf{r})$ of the particle density at the equilibrium density, $\rho_0(\mathbf{r})$.

$$\left. \frac{\delta E[\rho(\mathbf{r})]}{\delta\rho(\mathbf{r})} \right|_{\rho(\mathbf{r})=\rho_0(\mathbf{r})} = 0 \quad (2.9)$$

The model of Hohenberg–Kohn only tells us how to obtain the $\rho_0(\mathbf{r})$ without having to find the molecular wavefunction but it does not tell how to calculate the E_0 from $\rho_0(\mathbf{r})$. So, the next step of the DFT method has been carried out by Kohn and Sham in 1965. Based on the theory of Kohn–Sham, the density of a non–interacting n –electron system is assumed the same with the original molecular system. The total energy for DFT is then given as

$$E = E_T + E_V + E_J + E_{XC} \quad (2.10)$$

where

E_T is the kinetic energy of the non–interacting system

E_V is the attraction between the electrons and nuclei

E_J is the electron–electron repulsion energy (it is also called as the Hartree energy)

E_{XC} is the exchange–correction energy

The idea of finding energy as a function of electron density (Kohn and Sham, 1965) refers to the Thomas–Fermi model, which is developed in the end of 1920s. The electron density of the system is given by

$$N = \int \rho(\mathbf{r}) d\mathbf{r} \quad (2.11)$$

So, the attraction between the electrons and nuclei is written as

$$E_V = \sum_{A=1}^M \int \frac{Z_A}{|\mathbf{R}_A - \mathbf{r}|} \rho(\mathbf{r}) d\mathbf{r} \quad (2.12)$$

The electron–electron repulsion energy is given as

$$E_J = \frac{1}{2} \iint \frac{\rho(\mathbf{r}_1)\rho(\mathbf{r}_2)}{|\mathbf{r}_1 - \mathbf{r}_2|} d\mathbf{r}_1 d\mathbf{r}_2 \quad (2.13)$$

The kinetic energy density of the non–interacting system is defined by

$$E_T = a \int \rho^{\frac{5}{3}}(\mathbf{r}) d\mathbf{r} \quad (2.14)$$

The term of exchange–correlation energy is still remained unknown. However, there are several approximations for this term. The exchange–correlation energy is defined as

$$E_{XC}[\rho(\mathbf{r})] = \int f[\rho_\alpha(\mathbf{r}), \rho_\beta(\mathbf{r}), \nabla\rho_\alpha(\mathbf{r}), \nabla\rho_\beta(\mathbf{r})] d\mathbf{r} \quad (2.15)$$